

MEASURED AND CALCULATED STEADY AERODYNAMIC LOADS

ON A LARGE-SCALE UPPER-SURFACE BLOWN MODEL

Boyd Perry III
NASA Langley Research Center

Michael R. Mendenhall
Nielsen Engineering and Research, Inc.

SUMMARY

This paper presents static aerodynamic loads measurements from wind-tunnel tests of a full-scale upper-surface blown jet-flap configuration. The measured loads are compared with calculations using a recently developed method for predicting longitudinal aerodynamic characteristics of upper-surface blown jet-flap configurations.

INTRODUCTION

The performance and stability and control of upper-surface blown (USB) jet-flap configurations have been well documented. (See refs. 1 to 9.) These results have usually been presented as force and moment coefficients over the range of variables investigated, and most early models were small-scale and powered with compressed-air simulated engines. Some information has been published concerning detailed wing and flap load distributions. (See refs. 9 to 11.)

The development of analytical methods for predicting USB performance and loads has lagged behind the experimental work by 2 or 3 years. Such methods, which treat the aerodynamic interaction between lifting surfaces and the high-velocity exhaust wake, are now beginning to appear in the literature. (See refs. 12 to 14.)

In this paper, results of a loads investigation on a full-scale USB configuration powered with turbofan engines (presented previously in ref. 9) are presented. In addition, comparisons are made with calculated results based on an analytical method presently being developed under contract (which is an extension of the method of ref. 14). Measured wing and flap loads data are presented for parametric variations in angle of attack, flap deflection angle, and engine power setting, and for one engine inoperative.

SYMBOLS

Measurements and calculations were made in U.S. Customary Units and are presented in both the International System of Units (SI) and U.S. Customary Units.

- a' location of leading edge of Krueger flap projected onto wing reference plane and expressed as a fraction of local wing chord
- b' location of trailing edge of USB flap, double-slotted flap, or aileron, projected onto wing reference plane and expressed as a fraction of local wing chord
- b wing span, m (ft)
- C_p pressure coefficient, $\frac{P - P_\infty}{q_\infty}$
- C_μ static thrust coefficient, $\frac{T}{q_\infty S}$
- c local wing chord, m (ft)
- c_n section normal-force coefficient, $\int_{a'}^{b'} \Delta C_p d\left(\frac{x}{c}\right)$
- h initial height of rectangular vortex ring
- l initial width of rectangular vortex ring
- p local static pressure, N/m^2 (lb/ft²)
- p_∞ free-stream static pressure, N/m^2 (lb/ft²)
- q_∞ free-stream dynamic pressure, N/m^2 (lb/ft²)
- S wing area, m² (ft²)
- T static thrust force, N (lb)
- x chordwise coordinate, m (ft)
- y spanwise coordinate, m (ft)
- z vertical coordinate, m (ft)
- α angle of attack, deg
- δ_a aileron deflection, deg
- δ_f deflection of USB and double-slotted flap (deflected together), deg

Abbreviations:

BLC boundary-layer control

USB upper-surface blown

DESCRIPTION OF INSTRUMENTED MODEL

The model used in these tests is shown in the Langley full-scale tunnel in figure 1. The model had a wing span of 10.7 m (35.0 ft) and was equipped with two JT15D-1 turbofan engines (with nominal bypass ratio of 3.3). The high-lift system consisted of leading-edge Krueger flaps extending from the engine nacelles to the wing tips, leading-edge blowing boundary-layer control (BLC), upper-surface blown (USB) flaps extending from the fuselage to approximately 40 percent of the semispan, double-slotted flaps extending from approximately 40 percent to approximately 70 percent of the semispan, ailerons (capable of symmetrical deflection) extending from approximately 70 percent of the semispan to the wing tip, and aileron blowing BLC. The exhaust nozzle had an aspect ratio of 6.0 and a deflector attached to it to improve the spreading and turning of the jet exhaust. The right side of the model was instrumented with static pressure orifices at the eight spanwise stations indicated by the dashed lines in figure 1(a). A total of 270 pressure orifices were located on portions of the fuselage, wing, leading-edge Krueger flap, USB flap, double-slotted flap, and aileron. No static pressure orifices were located on the nacelle.

Chordwise sections taken at stations A, B, and C in figure 1(a) are shown in figure 1(b). The three sections are taken through the center of the engine, the double-slotted flap, and the aileron, respectively. Note that flap and aileron deflection angles are defined with respect to the wing reference plane indicated by the center line. A flap deflection of 32° and a symmetrical aileron deflection of 20° corresponds to a typical take-off configuration. A flap deflection of 72° and a symmetrical aileron deflection of 50° corresponds to a typical landing configuration.

ANALYTICAL PREDICTION METHOD

An analytical method, presently being developed under a NASA contract, was used to predict the static aerodynamic loads and the longitudinal aerodynamic characteristics of the USB configuration shown in figure 1. The method uses potential flow models to represent the lifting surfaces and engine wake and predicts the interference between these surfaces and the engine wake. The lifting surfaces are represented by a nonplanar vortex lattice and the engine by an expanding rectangular vortex "ring" model. Figure 2 illustrates the aerodynamic paneling scheme used to model the wing, flaps, and aileron. The shaded panels in figure 2 are those which receive direct interference from the engine wake. Figure 3 illustrates the simulated shape and location of the engine exhaust wake and the wake center line. The shape of the wake was empirically

tailored to the USB configuration of figure 1; that is, the width was determined by measuring the width of soot deposits from photographs in reference 9, and the height was determined from velocity profiles in reference 11 (which used the same engine and wing-flap as ref. 9). The rectangular vortex rings are normal to the wing and flap surfaces, resulting in a jet which is tangent to those surfaces. The wake center line moves aft at a constant y-station (see axis system in fig. 3) and it leaves the trailing edge of the last flap tangent to that surface. It then returns to the free-stream direction via a parabolic path at a distance equal to approximately 1 root chord downstream.

There are some limitations of the analytical prediction method which prevent complete simulation of the physical properties of the USB model. For example, the method cannot simulate either the exhaust nozzle deflector or leading-edge and aileron blowing BLC. In addition, there is no provision in the computer program for eliminating the contributions to the normal-force coefficient from that portion of the wing under the nacelles.

RESULTS AND DISCUSSION

Experimental Data

Figure 4 contains chordwise pressure distributions at a high thrust coefficient for the landing flap deflection. Shown is a portion of the nacelle and the upper surface of the wing and USB flap taken along chordwise section A of figure 1(a). The lines normal to the surface of the wing and flap indicate the location of static pressure orifices and the magnitudes of the pressures. The solid curve represents the wind-on condition (wind velocity was approximately 14 m/sec (45 ft/sec) at sea level), and the dashed curve represents the wind-off condition. Both distributions have the same general shape with about a 20-percent difference in magnitude. In both distributions the peak pressures occur at the knee of the flap. Also shown in the figure is a region of positive pressures at the point of exhaust impingement on the upper surface of the wing. The shapes of these pressure distributions are very similar to those shown in reference 10 and to those obtained in recent static tests of another large-scale USB model, in which peak pressures also occur at the knee of the flap.

Figures 5 to 8 contain plots of section normal-force coefficient c_n as a function of nondimensional semispan position $\frac{y}{b/2}$ for the present tests. Note that the location of the exhaust nozzle is identified in each of these figures. Since no pressure orifices were located on the nacelles, c_n does not include contributions from the nacelles. A common characteristic in figures 5 to 8 is the "dip" in the normal-force coefficient distributions. The dip occurs inboard of the nozzle center line and is due to positive pressures on the wing upper surface in the region of exhaust impingement. The positive pressures result in significantly lower section normal-force coefficients relative to adjacent spanwise stations, which have smaller positive pressures.

In figures 5 to 8, values of both section normal-force coefficient c_n and angle of attack α for constant values of thrust coefficient C_μ were obtained by interpolation of the basic corrected data.

Effect of engine thrust coefficient.- Figure 5 shows spanwise normal-force coefficient distributions for thrust coefficients of 0, 2.15, and 3.93. The angles of attack were 9.63° , 8.62° , and 7.95° , respectively (the difference in α has a negligible effect on the comparison). Examination of figure 5 indicates that from the fuselage center line to approximately 80 percent of the semispan the normal-force coefficients increased with increasing thrust coefficient. At the nozzle center line the normal-force coefficient for maximum thrust was an order of magnitude greater than that for zero thrust. Outboard, near the tip and well removed from the influence of the engine exhaust, the section normal-force coefficients for the two power-on conditions approached a common value, indicating that c_n is independent of C_μ near the tip.

Effect of angle of attack.- Figure 6 shows spanwise normal-force coefficient distributions for angles of attack of -1.3° , 8.5° , 18.3° , and 28.3° . This plot indicates that from the fuselage center line to a position slightly outboard of the nozzle, the spanwise normal-force coefficient is primarily dependent on the engine exhaust and shows little dependence on angle of attack. However, outboard of the nozzle the normal-force coefficient increases with increasing angle of attack as might be expected.

Effect of flap deflection angle.- Figure 7 shows spanwise normal-force coefficient distributions for flap deflection angles of 72° and 32° . The angles of attack were 8.48° for $\delta_f = 72^\circ$ and 8.03° for $\delta_f = 32^\circ$ (the difference in α has a negligible effect on the comparison). Examination of figure 7 indicates that the normal-force coefficients are consistently larger for the 72° flap setting than for the 32° flap setting. From near the tip to well within the spanwise extent of the exhaust nozzle, the normal-force coefficients for the 72° setting are consistently approximately twice as large as those for the 32° setting. Also of interest are c_n variations from the midpoint of the exhaust nozzle to slightly outboard of the exhaust nozzle. For the 72° flap deflection, maximum values of c_n occurred within the spanwise extent of the exhaust nozzle; for the 32° flap deflection, maximum values of c_n occurred outboard of the exhaust nozzle. The locations of these maximum values indicate that there was more spanwise spreading of the high-velocity exhaust for the smaller flap deflection angle than for the higher flap deflection angle.

Effect of one engine inoperative.- Figure 8 shows spanwise normal-force coefficient distributions on the right wing of the model for both engines operating, right engine only, left engine only, and both engines inoperative. The normal-force coefficient distributions for both engines operating and right engine only are very similar, with maximum variations in the region behind the exhaust nozzle. The spanwise normal-force coefficient distributions for left engine only and both engines inoperative are almost identical, indicating that there is very little lift carryover for this model. This result is not in agreement with results from other USB configurations with one engine inoperative (for example, see ref. 10). One reason for the absence of lift carryover for

the present model could be severe flow separation on the fuselage due to the interference between the fuselage and nacelles (ref. 9). It is believed that a leading-edge Krueger flap between the fuselage and nacelles could provide attached flow in this region and therefore provide better flow conditions for lift carryover with one engine inoperative, as indicated by some unpublished data recently obtained.

Analytical Comparison

Some preliminary analytical results obtained by using the prediction method mentioned previously are presented in this section of the paper and compared with experimental data. Figure 9 contains comparisons of experimental and analytical spanwise normal-force coefficient distributions at three power settings for a flap deflection of 72° . Measurements were made at 8 spanwise locations, and analytical calculations were performed at 16 locations. For $C_{\mu} = 0$ (in the upper left side of fig. 9) there is good agreement between predicted and measured results outboard of the nozzle. The predicted loads are too high in the nozzle region. As stated previously, some of this difference may be explained by the lifting surface model in the current program. The wing in the nacelle region is represented with a vortex-lattice arrangement and is allowed to carry loads as if the nacelle were not present. Therefore, this procedure must be permitting too much load to be carried by the wing in this region. For power-on conditions (in the lower left and lower right sides of fig. 9) the theoretically predicted normal-force coefficient distributions show reasonably good agreement with the experimental results. The peak loads for both theoretical and experimental results occur within the spanwise extent of the exhaust nozzle; however, the theoretical peak loads are approximately 20 percent higher. Part of this difference is due to the static pressure differences just mentioned. Another factor contributing to the difference is that the actual flow is highly complex in this region, with areas of positive and negative pressures on the wing upper surface. The analytical prediction method cannot simulate this effect. Outboard, near the wing tip and away from the influence of the engine exhaust, the theoretical and experimental results agree more closely.

CONCLUDING REMARKS

Static pressures were measured on the fuselage, Krueger flap, wing, upper-surface blown (USB) flap, double-slotted flap, and aileron of a large-scale USB model equipped with turbofan engines. Section normal-force coefficients were determined from static pressure data. The power-on section normal-force coefficients directly behind the exhaust nozzle were about an order of magnitude larger than the power-off coefficients at the same location. The section normal-force coefficients were insensitive to angle of attack within the spanwise extent of the exhaust nozzle, but very sensitive to both flap deflection angle and thrust coefficient. Greater spanwise spreading was observed with the flaps deflected for the take-off configuration (32°) than for the landing configuration (72°). For one engine inoperative, there was very little lift carryover across the fuselage for this model.

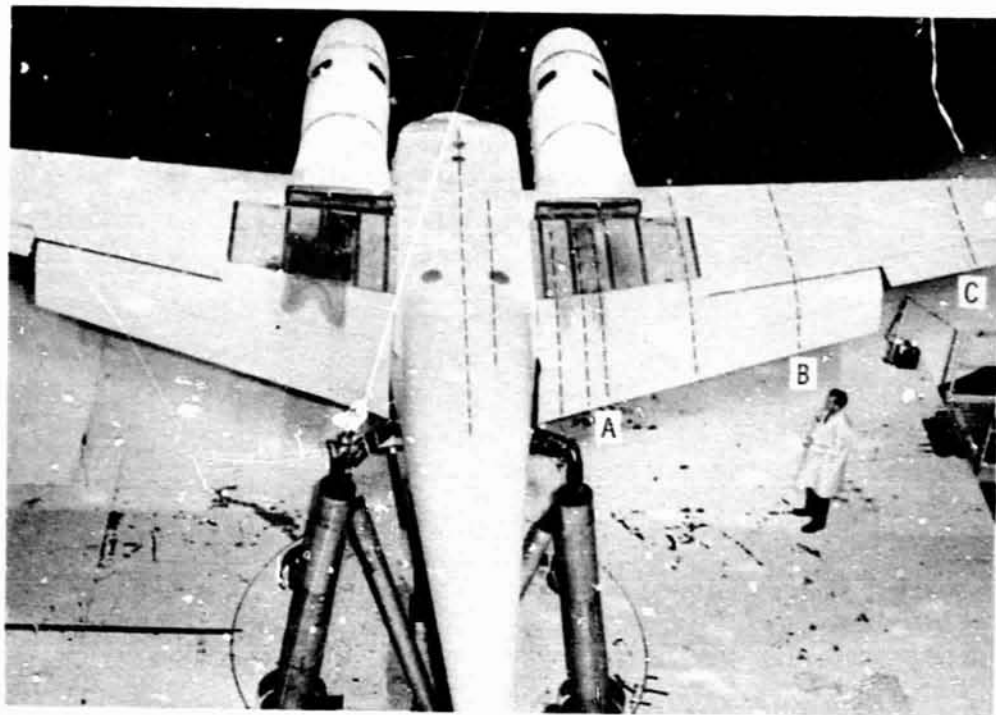
Some experimental data were compared with analytical results of a method presently being developed under contract. Preliminary results from this method indicate that the analytically predicted shape of the spanwise distribution of section normal-force coefficients is correct, but the magnitudes are approximately 20 percent high for the power-on conditions.

REFERENCES

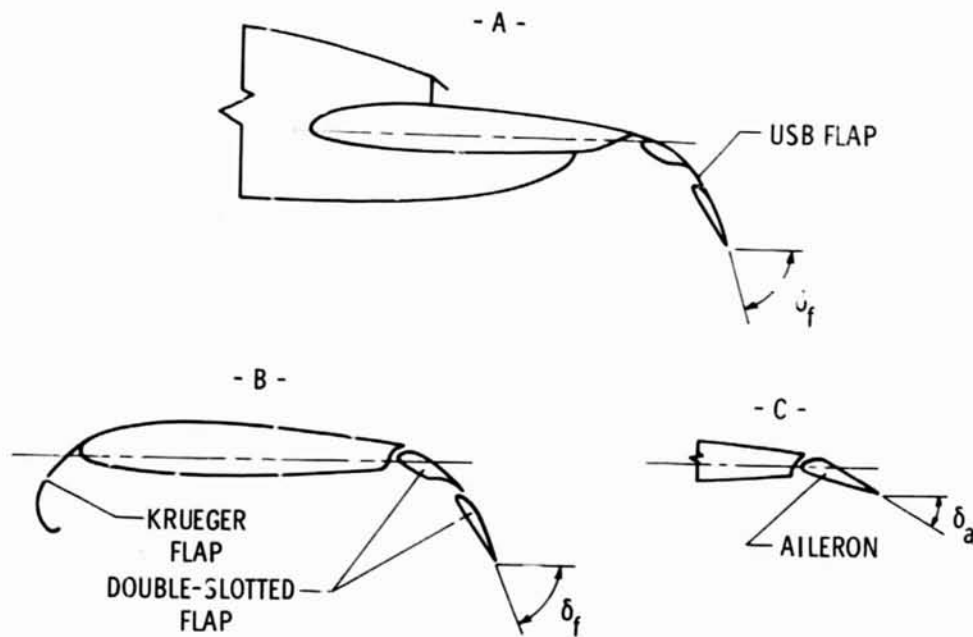
1. Phelps, Arthur E.; Letko, William; and Henderson, Robert L.: Low-Speed Wind-Tunnel Investigation of a Semispan STOL Jet Transport Wing-Body With an Upper-Surface Blown Jet Flap. NASA TN D-7183, 1973.
2. Phelps, Arthur E., III; and Smith, Charles C., Jr.: Wind-Tunnel Investigation of an Upper Surface Blown Jet-Flap Powered-Lift Configuration. NASA TN D-7399, 1973.
3. Aoyagi, Kiyoshi; Falarski, Michael D.; and Koenig, David G.: Wind Tunnel Investigation of a Large-Scale Upper Surface Blown-Flap Transport Model Having Two Engines. NASA TM X-62,296, 1973.
4. Aoyagi, Kiyoshi; Falarski, Michael D.; and Koenig, David G.: Wind Tunnel Investigation of a Large-Scale Upper Surface Blown-Flap Model Having Four Engines. NASA TM X-62419, 1975.
5. Carros, Robert J.; Boissevain, Alfred G.; and Aoyagi, Kiyoshi: Aerodynamic Characteristics of a Large-Scale Hybrid Upper Surface Blown Flap Model Having Four Engines. NASA TM X-62460, 1975.
6. Smith, Charles C., Jr.; Phelps, Arthur E., III; and Copeland, W. Latham: Wind-Tunnel Investigation of a Large-Scale Semispan Model With an Unswept Wing and an Upper-Surface Blown Jet Flap. NASA TN D-7526, 1974.
7. Parlett, Lysle P.: Free-Flight Wind-Tunnel Investigation of a Four-Engine Sweptwing Upper-Surface Blown Transport Configuration. NASA TM X-71932, 1974.
8. Phelps, Arthur E., III: Wind-Tunnel Investigation of a Twin-Engine Straight-Wing Upper-Surface Blown Jet-Flap Configuration. NASA TN D-7778, 1975.
9. Staff of Langley Research Center: Wind-Tunnel Investigation of the Aerodynamic Performance, Steady and Vibratory Loads, Surface Temperatures and Acoustic Characteristics of a Large-Scale Twin-Engine Upper-Surface Blown Jet-Flap Configuration. NASA TM X-72794, 1975.
10. Smith, Charles C., Jr.; and White, Lucy C.: Pressure Distribution of a Twin-Engine Upper-Surface Blown Jet-Flap Model. NASA TM X-71937, 1974.
11. Shivers, James P.; and Smith, Charles C., Jr.: Static Tests of a Simulated Upper Surface Blown Jet-Flap Configuration Utilizing a Full-Size Turbofan Engine. NASA TN D-7816, 1975.
12. Lan, C. Edward; and Campbell, James F.: Theoretical Aerodynamics of Upper-Surface-Blowing Jet-Wing Interaction. NASA TN D-7936, 1975.

13. Lan, C. Edward: A Theoretical Investigation of Over-Wing-Blowing Aerodynamics. NASA CR-144969, 1976.

14. Mendenhall, M. R.; Perkins, S. C., Jr.; Goodwin, F. K.; and Spangler, S. B.: Calculation of Static Longitudinal Aerodynamic Characteristics of STOL Aircraft With Upper-Surface-Blown Flaps. NASA CR-137646, 1975.



(a) Model in Langley full-scale tunnel.



(b) Chordwise sections.

Figure 1.- Test configuration.

REPRODUCIBILITY OF THE ORIGINAL PAGE IS POOR

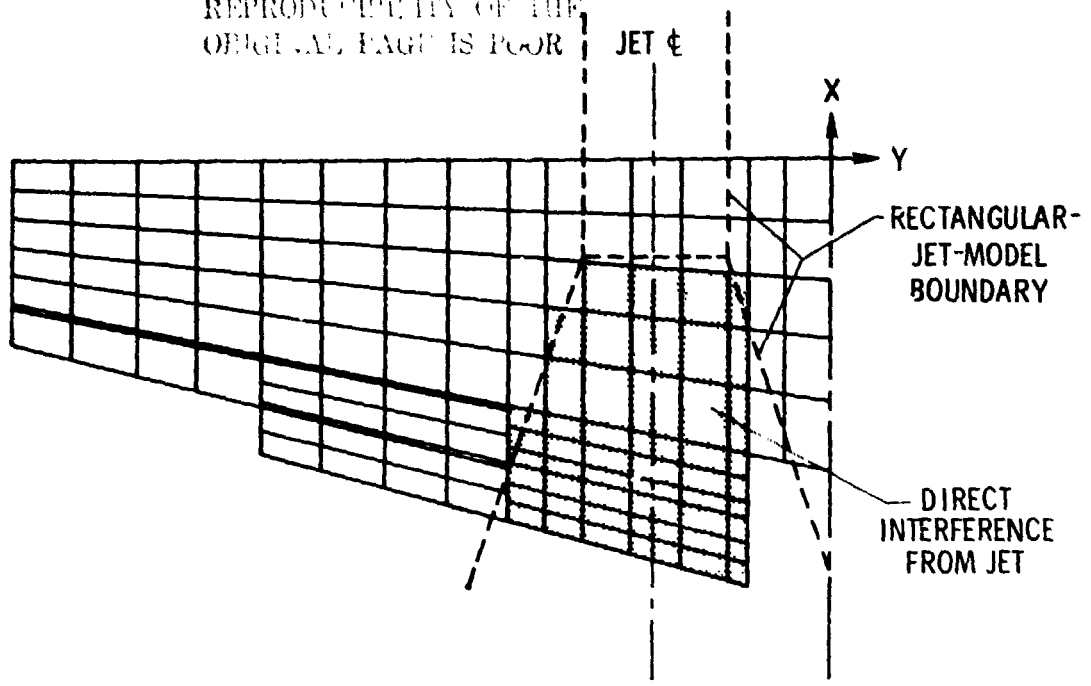


Figure 2.- Vortex-lattice layout.

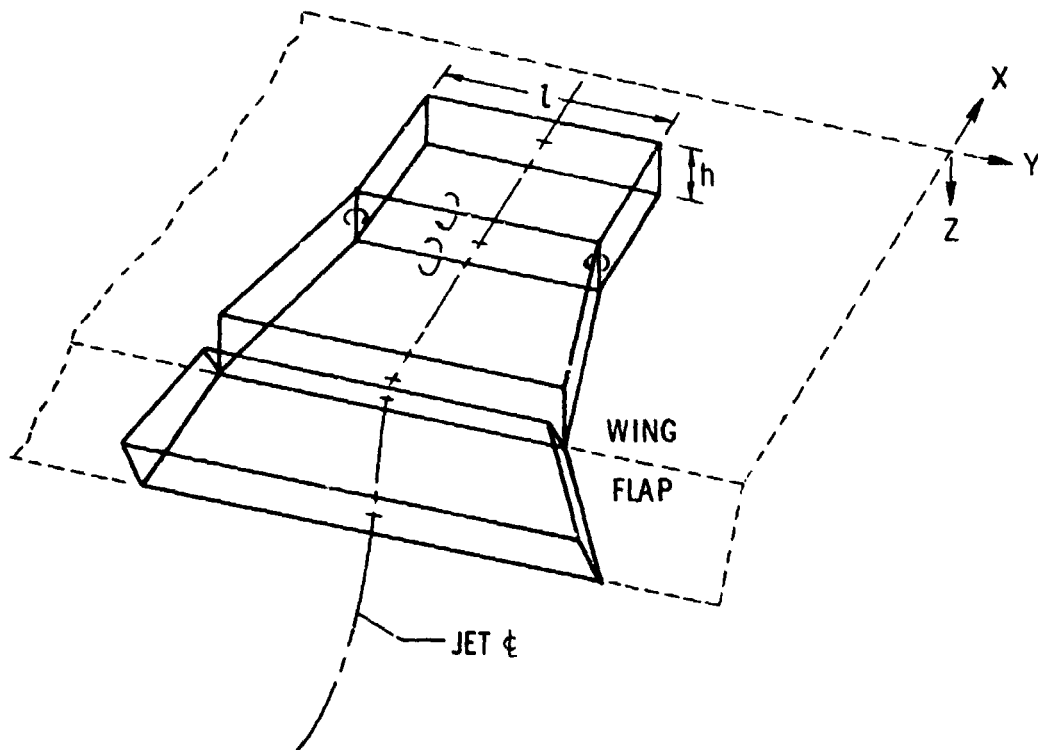


Figure 3.- Rectangular vortex ring jet model.

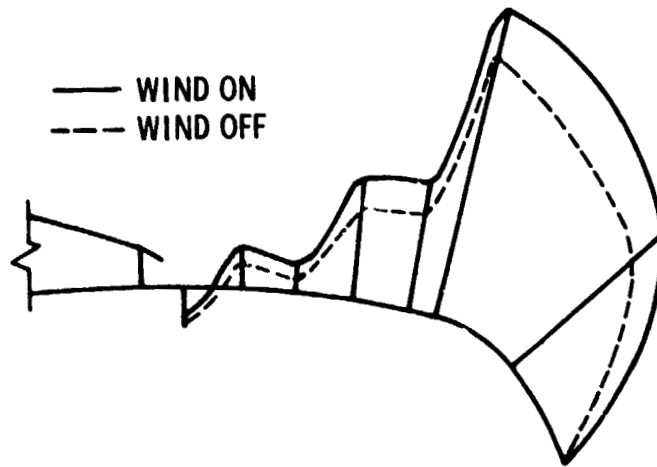


Figure 4.- Chordwise static pressure distributions along engine center line. $C_{\mu} = 3.93$; $\delta_f = 72^\circ$.

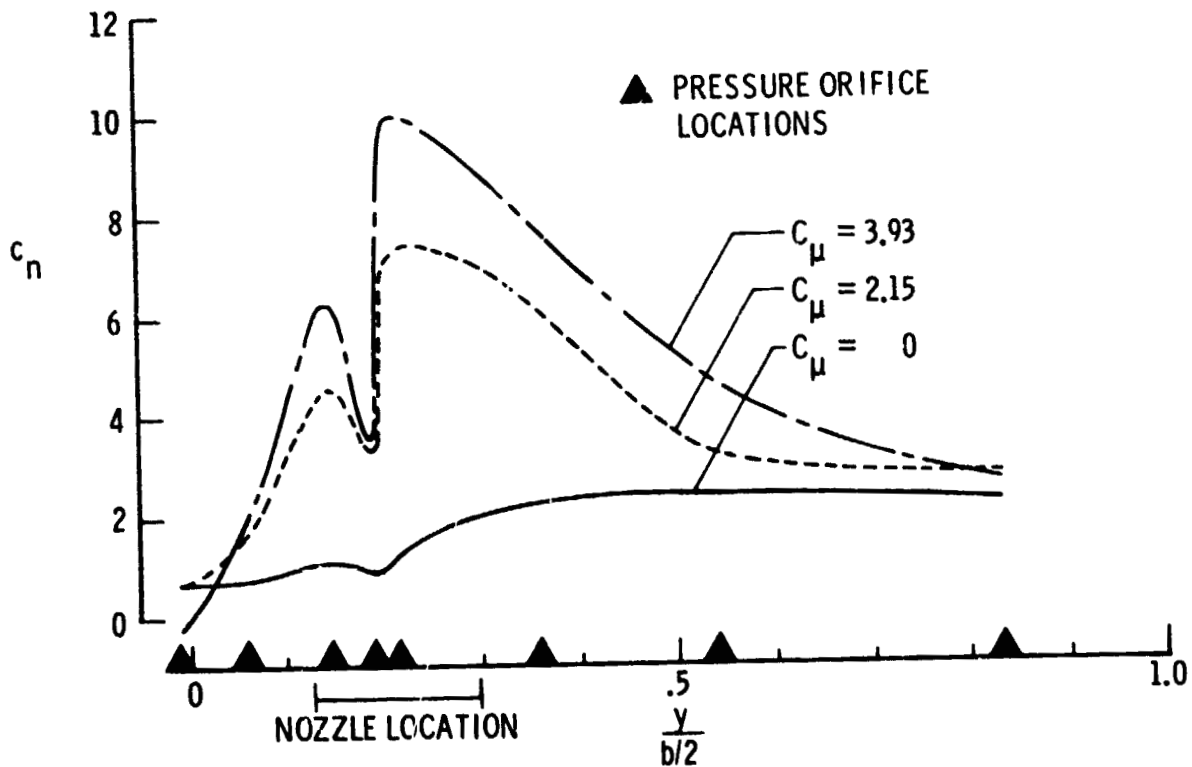


Figure 5.- Effect of thrust coefficient on spanwise loads. $\alpha = 10^\circ$ (nominal); $\delta_f = 72^\circ$; $\delta_a = 50^\circ$.

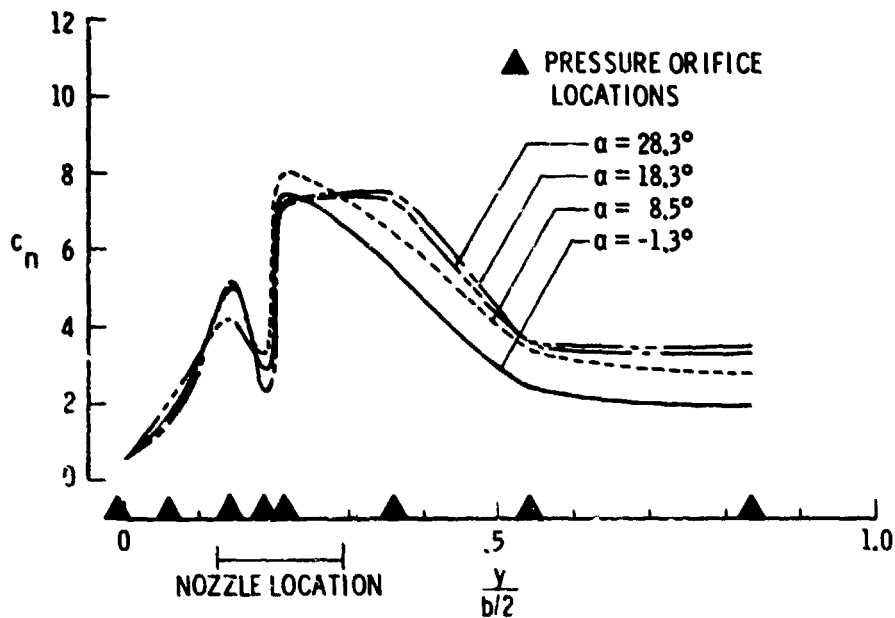


Figure 6.- Effect of angle of attack on spanwise loads.
 $C_{\mu} = 2.5$; $\delta_f = 72^\circ$; $\delta_a = 50^\circ$.

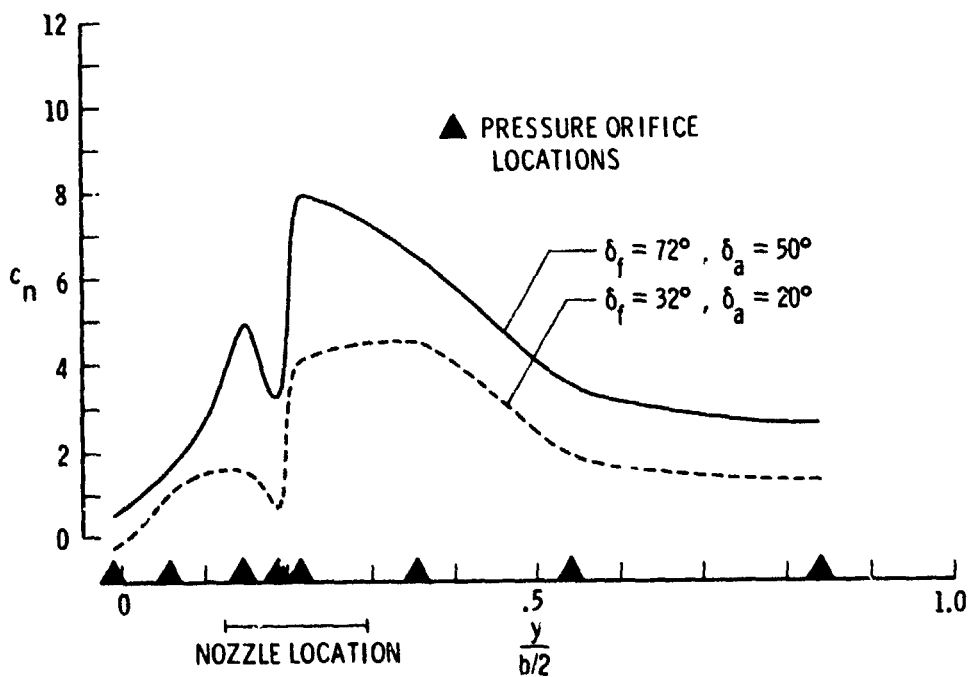


Figure 7.- Effect of flap deflection on spanwise loads.
 $C_{\mu} = 2.5$; $\alpha = 10^\circ$ (nominal).

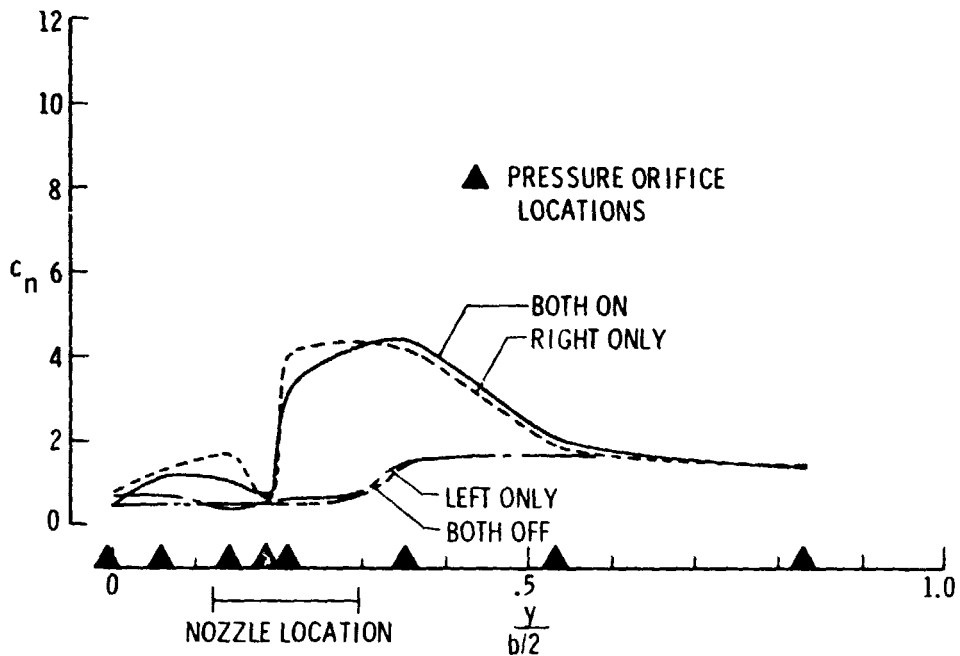


Figure 8.- Effect of one engine inoperative on spanwise loads on right wing. $\alpha = 10^\circ$ (nominal); $\delta_f = 32^\circ$; $\delta_a = 20^\circ$; $C_\mu = 1.0$ per engine.

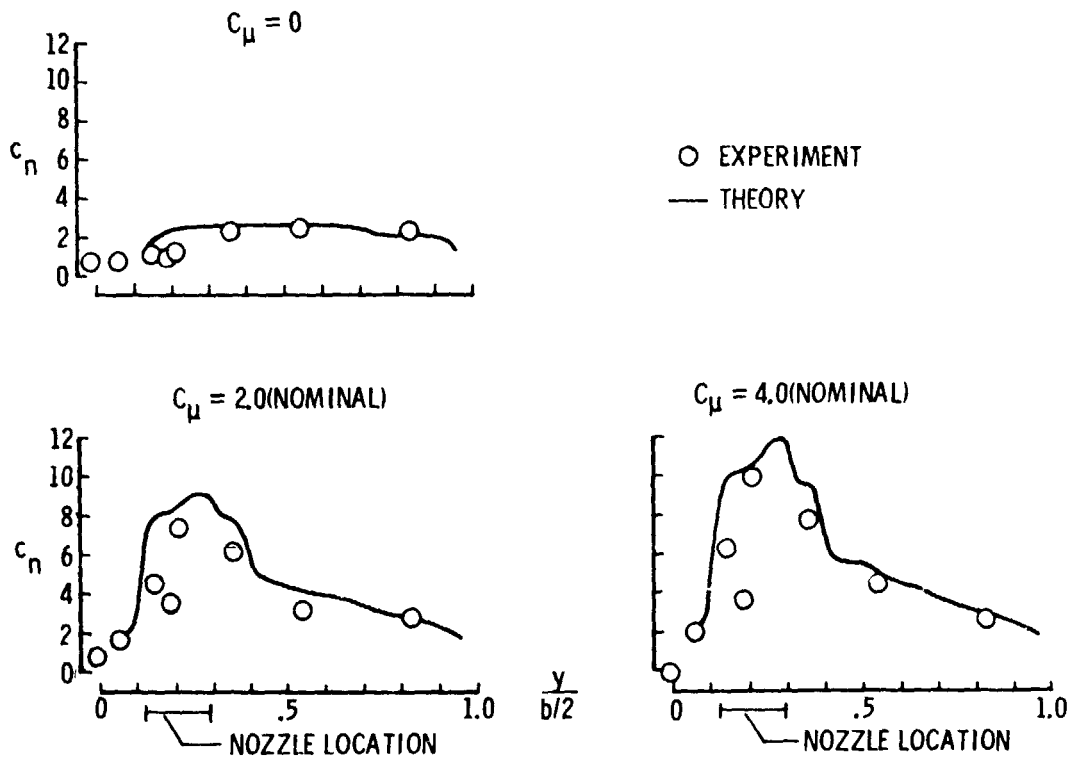


Figure 9.- Measured and calculated spanwise loads. $\alpha = 10^\circ$ (nominal); $\delta_f = 72^\circ$; $\delta_a = 50^\circ$.